

Inverse Design Method Starting for Aperture Field from Phaseless Radiation Pattern Based on Spectral Analysis

Chuan-Sheng Chen, Ren Wang, *Member, IEEE*, Jin-Pin Liu, and Bing-Zhong Wang, *Senior Member, IEEE*

This work has been submitted to the IEEE for possible publication. Copyright may be transferred without notice, after which this version may no longer be accessible.

Abstract—Existing electromagnetic inverse design methods are often established in the spacial domain. This communication presents an inverse design method, which can design aperture field for the desired phaseless radiation pattern, from the spectral domain perspective. In addition, it naturally adapts to the polarization constraint. Specifically, the inverse design can be converted into solving the first kind of Fredholm integral equation, using the spectral domain method. To deal with the ill-posedness of such integral equation, we apply modal expansion to the integrand. To cope with the non-linearity introduced by phaseless, we use a multi-objective optimization algorithm to obtain the coefficients in the modal expansion. Finally, we use this method to break the cosine rule that the directivity of 2D arrays drops as cosine of the angle, which is a puzzle in wide-angle scanning. The numerical simulation results meet expectations and illustrate the feasibility of the method.

Index Terms—inverse problem; spectral domain method; aperture field; radiation pattern

I. INTRODUCTION

THE radiation pattern of antennas are always guided by the requirements of electromagnetic systems. However, existing design methods are either only applicable to specific antennas, which do not have good universality [1], [2], or use optimization to achieve simple requirements which lack flexibility [3], [4]. A general design method for arbitrary radiation pattern, especially phaseless pattern is worth studying. The main difficulty is how to effectively handle the non-linearity introduced by phaseless. In addition, the polarization criteria of the radiation pattern should not be ignored. Obviously, the design problem starting from phaseless arbitrary pattern is a typical inverse design problem that aims to find an unknown *cause* from its known *effect* [5].

In fact, inverse design has gradually been favored by scholars [6]–[10]. The inverse source framework presented in [9] is based on the well-known electric field integral equation (EFIE), and belongs to the spacial domain analysis, as shown in (1). A conjugate gradient (CG) algorithm [11] is used to iteratively update \mathbf{J} and \mathbf{M} to solve the integral equation. Based on this framework, [10] used the three-layer admittance model to design a metasurface for one desired radiation pattern.

Manuscript received on Nov 27, 2022. This work was supported in part by the National Natural Science Foundation of China under Grants 62171081 and 61901086. (*Corresponding authors: Bing-Zhong Wang.*)

All four authors are with the Institute of Applied Physics, University of Electronic Science and Technology of China (UESTC), Chengdu, 611731, China, (e-mail: cschen1997@gmail.com, rwang@uestc.edu.cn, jpinliu@gmail.com, and bzwang@uestc.edu.cn).

$$\mathcal{G}(\mathbf{J}, \mathbf{M}) = -j\eta_0 k_0 \int_{\Sigma^+} \left[\mathbf{J}(\mathbf{r}') + \frac{1}{k_0^2} \nabla \nabla'_s \cdot \mathbf{J}(\mathbf{r}') \right] g(\mathbf{r}, \mathbf{r}') ds' - \nabla \times \int_{\Sigma^+} \mathbf{M}(\mathbf{r}') g(\mathbf{r}, \mathbf{r}') ds' \quad (1)$$

The spacial domain framework proposed in [9] has good generality. However, when the design target is phaseless pattern, some calculations in (1) may be redundant. This part of the computational burden is not negligible during the iterative solution. In addition, the applicability of CG algorithm to non-linear problems remains to be discussed. When dealing with dual polarization constraints, it is irregular but important to balance the weights of different polarizations in the objective function.

This communication proposes an inverse design method which can deal with the phaseless pattern well. It reduces the computational burden by combining the far-field asymptotics of the spectral domain method, and is naturally adapt different polarization constraint by combining with the coordinate transformation. We use multi-objective optimization algorithms to deal with the non-linearity introduced by phaseless. To illustrate the significance of our method, we use it to break the cosine rule that the directivity of 2D arrays drops as cosine of the scanning angle, and the numerical results show that we succeeded.

The rest of this communication is presented as follows. Section II introduces the basic forward problem. Section III introduces the inverse design methodology, which ultimately translates the inverse design problem into solving the first kind of two dimensional Fredholm integral equation. Section IV analyses how to solve the integral equations, and Section V demonstrates the capability of the method through an example breaking the cosine rule.

II. FORWARD PROBLEM STATEMENT

The general aperture radiation problem is calculating the radiation field from the known aperture field $\mathbf{E}_{\text{ape}}(x, y)|_{z=0}$. Its schematic diagram is shown in Fig. 1. The analysis below consider only the upper half-space ($z > 0$), that is $\theta \in [0, \pi/2]$. \mathbf{E}_{ape} , which has a definition domain $\{(x, y) | x \in [-a/2, a/2], y \in [-b/2, b/2]\}$, locate in the infinite PEC plane ($z = 0$ plane). According to the uniqueness theorem, as long as the tangential components of $\mathbf{E}_{\text{ape}}(x, y)$ ($E_{\text{ape},x}$ and $E_{\text{ape},y}$) are known, $\mathbf{E}(x, y, z)|_{z>0}$ is uniquely

determined. This forward problem can be analyzed from the spatial or spectral domains.

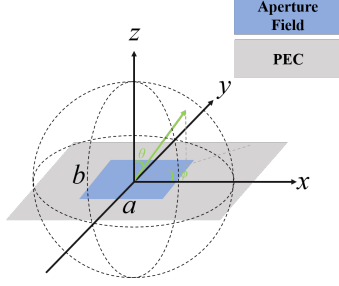


Fig. 1. Schematic diagram of the general forward aperture problem

In the spatial domain analysis, it can be transformed into a problem of magnetic current ($\mathbf{M}_s = -2\mathbf{n} \times \mathbf{E}_a$) radiation in free space [12]. $\mathbf{E}(x, y, z)|_{z>0}$ can be calculated by using the Green's function method shown in (1) or by introducing the auxiliary potential functions \mathbf{A} and \mathbf{F} .

In the spectral domain, as written in (2), the monochromatic wave field $\mathbf{E}(x, y, z)$ radiated by the aperture can be regarded as a superposition of plane waves of the form $\mathbf{f}(\theta, \phi) \exp(-j\mathbf{k} \cdot \mathbf{r})$ [13].

$$\mathbf{E}(x, y, z) = \frac{1}{4\pi^2} \int_{-\infty}^{\infty} \int_{-\infty}^{\infty} \mathbf{f}(\theta, \phi) e^{-j\mathbf{k} \cdot \mathbf{r}} dk_x dk_y \quad (2)$$

where $k_x = k \sin \theta \cos \phi$, $k_y = k \sin \theta \sin \phi$, and $k_z^2 = k^2 - k_x^2 - k_y^2$. f_x and f_y are given by (3) and are the components of \mathbf{f} .

$$f_x(\theta, \phi) = \int_{-\frac{b}{2}}^{\frac{b}{2}} \int_{-\frac{a}{2}}^{\frac{a}{2}} E_{\text{ape},x}(x', y') \cdot e^{j(k_x x' + k_y y')} dx' dy' \quad (3a)$$

$$f_y(\theta, \phi) = \int_{-\frac{b}{2}}^{\frac{b}{2}} \int_{-\frac{a}{2}}^{\frac{a}{2}} E_{\text{ape},y}(x', y') \cdot e^{j(k_x x' + k_y y')} dx' dy' \quad (3b)$$

The far-field asymptotic evaluation of (2) is (4), by using the *Stationary Phase* method.

$$\mathbf{E}(r, \theta, \phi) \approx j \frac{ke^{-jkr}}{2\pi r} \mathbf{e}_{\text{far}}(\theta, \phi) \quad (4a)$$

$$\begin{aligned} \mathbf{e}_{\text{far}}(\theta, \phi) &= \hat{\mathbf{a}}_{\theta} e_{\text{far},\theta}(\theta, \phi) + \hat{\mathbf{a}}_{\phi} e_{\text{far},\phi}(\theta, \phi) \\ &= \hat{\mathbf{a}}_{\theta} (f_x \cos \phi + f_y \sin \phi) \\ &\quad + \hat{\mathbf{a}}_{\phi} [\cos \theta (-f_x \sin \phi + f_y \cos \phi)] \end{aligned} \quad (4b)$$

In most cases, we pay more attention to the pattern $e_{\text{far}}(\theta, \phi)$ than $j \frac{ke^{-jkr}}{2\pi r}$, the coefficient on distance. Obviously, the e_{far} here includes both polarization and phase information.

III. INVERSE DESIGN METHODOLOGY

This section focuses on how to introduce phaseless pattern into the existing formulations, so as to convert phaseless pattern targets into constraints on aperture field. It is important to emphasize that, during the inverse design process, the given is the phaseless pattern $|e_{\text{far},\theta}|$ and $|e_{\text{far},\phi}|$, which can not be directly brought into (5).

$$f_x(\theta, \phi) = e_{\text{far},\theta}(\theta, \phi) \cos \theta - e_{\text{far},\phi}(\theta, \phi) \sin \phi / \cos \theta \quad (5a)$$

$$f_y(\theta, \phi) = e_{\text{far},\theta}(\theta, \phi) \sin \phi + e_{\text{far},\phi}(\theta, \phi) \cos \phi / \cos \theta \quad (5b)$$

So we obtain (6) by taking modulus of both sides of (5). γ in (6) is a function of θ and ϕ , which represents the phase difference of two polarization components at a certain direction (θ, ϕ) .

$$|f_x(\theta, \phi)| = \sqrt{\frac{|e_{\text{far},\theta}|^2 \cos^2 \theta + |e_{\text{far},\phi}|^2 \sin^2 \phi / \cos^2 \theta}{-2|e_{\text{far},\theta}| |e_{\text{far},\phi}| \sin \phi \cos \gamma}} \quad (6a)$$

$$|f_y(\theta, \phi)| = \sqrt{\frac{|e_{\text{far},\theta}|^2 \sin^2 \theta + |e_{\text{far},\phi}|^2 \cos^2 \phi / \cos^2 \theta}{+2|e_{\text{far},\theta}| |e_{\text{far},\phi}| \sin \phi \cos \phi / \cos \theta \cos \gamma}} \quad (6b)$$

Combined with engineering applications, we also give another expression of (6) for horizontal and vertical polarization ($|e_{\text{far},h}|$ and $|e_{\text{far},v}|$), by using *Ludwig3* coordinate system, as shown in (7).

$$|f_x(\theta, \phi)| = \sqrt{|l_1|^2 + |l_2|^2 + 2|l_1||l_2| \cos \gamma} \quad (7a)$$

$$|f_y(\theta, \phi)| = \sqrt{|l_3|^2 + |l_4|^2 + 2|l_3||l_4| \cos \gamma} \quad (7b)$$

where

$$l_1 = e_{\text{far},h} (\cos^2 \phi + \sin^2 \phi / \cos \theta);$$

$$l_2 = e_{\text{far},v} \sin \phi \cos \phi (1 - 1/\cos \theta);$$

$$l_3 = e_{\text{far},h} \sin \phi \cos \phi (1 - 1/\cos \theta);$$

$$l_4 = e_{\text{far},v} (\sin^2 \phi + \cos^2 \phi / \cos \theta);$$

Several common cases regarding (7) are discussed next.

- **Case I: Linear Polarization**

When only a single polarization is needed, another orthogonal polarization can be set to 0. For example, when only the vertical polarization $e_{\text{far},v}$ is considered, (7) degenerates to (8).

$$|f_x(\theta, \phi)| = |l_2|; |f_y(\theta, \phi)| = |l_4| \quad (8)$$

- **Case II: Circular Polarization**

Circular polarization requires that the modulus values of the two polarization components are equal, and the phase difference is 90° . That is $|e_{\text{far},h}| = |e_{\text{far},v}|$, and $\gamma = 90^\circ$ in any direction (θ, ϕ) . Then, (7) degenerates to (9).

$$|f_x(\theta, \phi)| = \sqrt{|l_1|^2 + |l_2|^2}; |f_y(\theta, \phi)| = \sqrt{|l_3|^2 + |l_4|^2} \quad (9)$$

- **Case III: Elliptical Polarization**

Once γ is determined, equation (7) itself corresponds to elliptical polarization.

The $|f_x|$ and $|f_y|$ in (6) and (7) act as bridges to deliver the phaseless pattern constraints to the aperture field constraints. Hence, the problem of solving the aperture field can be summarized in two steps:

- 1) Get $|f_x|$ and $|f_y|$ from the desired $|e_{\text{far},\theta}|$ and $|e_{\text{far},\phi}|$ or $|e_{\text{far},h}|$ and $|e_{\text{far},v}|$ by using (6) or (7).
- 2) Find a suitable set of solutions ($E_{\text{ape},x}$ and $E_{\text{ape},y}$) from $|f_x|$ and $|f_y|$ according to (10).

$$|f_x(\theta, \phi)| = \left| \int_{-\frac{b}{2}}^{\frac{b}{2}} \int_{-\frac{a}{2}}^{\frac{a}{2}} E_{\text{ape},x}(x', y') \cdot e^{j(k_x x' + k_y y')} dx' dy' \right| \quad (10a)$$

$$|f_y(\theta, \phi)| = \left| \int_{-\frac{b}{2}}^{\frac{b}{2}} \int_{-\frac{a}{2}}^{\frac{a}{2}} E_{\text{ape},y}(x', y') \cdot e^{j(k_x x' + k_y y')} dx' dy' \right| \quad (10b)$$

During Step 2, the inverse Fourier transform can not be used in (10). The root cause is the non-linearity introduced by the phaseless. Therefore, we can only treat (10) as the first kind of two-dimensional Fredholm integral equations after the modulo operation, which is difficult to obtain analytical solutions [14].

IV. SOLVING INTEGRAL EQUATION FOR APERTURE FIELD

This section describes how to solve the integral equation (10), in this electromagnetic inverse problem.

A. Modal Expansion on Aperture Field

Since directly solving the integral equation is difficult, we expand the unknown integrand \mathbf{E}_{ape} using the modal expansion method. Specifically, \mathbf{E}_{ape} satisfies the boundary conditions (12), as can be seen from Fig. 1.

$$\begin{cases} E_{\text{ape},x}|_{y=-\frac{b}{2}, \frac{b}{2}} = 0 \\ E_{\text{ape},y}|_{x=-\frac{a}{2}, \frac{a}{2}} = 0 \end{cases} \quad (12)$$

Equation (11) convert the problem of solving $\mathbf{E}_{\text{ape}}(x, y)$ to solving the unknown complex modal coefficients α_{mn}^i and β_{mn}^i , ($i = x, y$). The selection of the basis function is not unique. The trigonometric functions were chosen because they are the harmonic functions of the waveguide harmonic equation, if we regard the modal shown in Fig. 1 as a waveguide connected to the infinite PEC plane. Due to the existence of the analytic expression, (11) can use an analytical integration instead of numerical integration, which improves computational efficiency. The analytical integration of (11) is given in Appendix A.

B. Obtain Modal Coefficients by Using MOO

We obtain α_{mn}^i and β_{mn}^i ($i = x, y$) by using the multi-objective optimization algorithm(MOO). Here we use *the PSO toolbox*, and define (13) as the objective function of MOO,

$$\text{obj} = 1 - \frac{\text{cov}(\mathcal{N}(|\mathbf{f}_{\text{tar}}(\theta, \phi)|), \mathcal{N}(|\mathbf{f}_{\text{cal}}(\theta, \phi)|))}{\sigma_{\mathcal{N}(|\mathbf{f}_{\text{tar}}(\theta, \phi)|)} \cdot \sigma_{\mathcal{N}(|\mathbf{f}_{\text{cal}}(\theta, \phi)|)}} \quad (13)$$

where cov denotes the covariance of two vectors, the operator \mathcal{N} represents unfolding a two-dimensional matrix into a one-dimensional vector, $|\mathbf{f}_{\text{tar}}|$ is known from (6) and (7), and \mathbf{f}_{cal} is calculated from the optimized α_{mn}^y and β_{mn}^y . The choice of objective function is not unique and can be selected according to the design requirements.

V. NUMERICAL SIMULATION

This section shows numerical experiments using the above method to implement a specific $|e_{\text{tar}}|$. To illustrate the significance of our method, we use it to an example breaking the cosine rule.

A. Specially selected design targets

It is well known that when scanning to 60 degrees, the directivity of the 2D array factor is half of that at broadside. This is the cosine rule in wide-angle scanning [15].

Take a uniform amplitude broadside 16×16 dipole array with elements spaced at $\lambda/2$ distributed in the xoy plane as an example, its three-dimensional radiation pattern is shown in Fig. 2(a), denoted as $|e_{\text{tar},0^\circ}|$. The directivity of the dipole array is 25.29 dBi and decreases as the scan angle increases, as shown by the solid line in Fig. 3. The dashed line in Fig. 3 represents the results according to the cosine rule.

First, we need a set of design targets. We obtain it by rotating the coordinate system. And this set of target pattern has different beam direction angle but the same directivity of 25.29 dBi, which does not conform to the cosine rule, as shown in Fig. 2(b, c, d). Assume that the polarization is linear and only vertical, set (14) according to case I in section III.

$$|e_{\text{tar},\text{scan_degree},v}| = |e_{\text{tar},\text{scan_angle}}| \quad (14a)$$

$$e_{\text{tar},\text{scan_angle},h} = 0 \quad (14b)$$

Once targets are determined, the first step is to calculate $|f_x|$ and $|f_y|$ by using (8). Here, we only consider $|f_y|$, this is because the calculated $|f_x|$ are approximately 0. Thus, the aperture field has only $E_{\text{ape},y}$, but no $E_{\text{ape},x}$.

B. Numerical Simulation Settings

Next step is solving $E_{\text{ape},y}$ (more precisely, obtaining α_{mn}^y and β_{mn}^y) from $|f_y|$ according to (15b) by using MOO.

In the following numerical simulation, the size of the aperture is set to $7.5\lambda \times 7.5\lambda$, as the 16×16 array. That is, the dimension of aperture a and b are set to be 7.5λ . The mode numbers M and N are set to be 8 at small scanning angles and are set to be 16 at more than 45° . Fewer modes would introduce low design freedom, resulting in failure to achieve targets. Too many modes increase the computational burden and make the calculated aperture field vary dramatically. Such oscillation is not expected and is difficult to achieve. There has to be a tradeoff, and an acceptable approach is that the shortest modal wavelength is less than half of the operating wavelength. This makes the oscillation easy to realize in physics. θ and ϕ need to be divided into appropriate steps according to the fluctuation of the target pattern. Here, θ from 0 to $\pi/2$ and ϕ from 0 to 2π are divided into 45 and 180 parts.

C. Numerical Simulation Results

The normalized amplitude and phase distribution of aperture field calculated by this method are shown in Fig. 4. To verify the correctness, we use a script to construct $E_{\text{ape},y}$ and excite it in *CST Microwave Studio*. The full-wave simulation results are shown in Fig.5, the directivity of the four sub-pictures is 25.29 dBi, 25.29 dBi, 25.24 dBi, and 24.14 dBi, respectively.

We have also done numerical simulation for other scanning angles and summarized their directivity in the dot-dash line in Fig. 3. So far, we have successfully inverse designed a series of aperture field, the directivity of which break the cosine rule. This fully demonstrates the significance of the method.

$$|f_x(\theta, \phi)| = \left| \int_{-\frac{b}{2}}^{\frac{b}{2}} \int_{-\frac{a}{2}}^{\frac{a}{2}} \left\{ \sum_{n=1}^N \left[\left(\sum_{m=1}^M \alpha_{mn}^x \sin\left(\frac{m\pi}{a}(x' + \frac{a}{2})\right) + \sum_{m=0}^M \beta_{mn}^x \cos\left(\frac{m\pi}{a}(x' + \frac{a}{2})\right) \right) \sin\left(\frac{n\pi}{b}(y' + \frac{b}{2})\right) \right] \right\} e^{j(k_x x' + k_y y')} dx' dy' \right| \quad (11a)$$

$$|f_y(\theta, \phi)| = \left| \int_{-\frac{b}{2}}^{\frac{b}{2}} \int_{-\frac{a}{2}}^{\frac{a}{2}} \left\{ \sum_{m=1}^M \left[\left(\sum_{n=1}^N \alpha_{mn}^y \sin\left(\frac{n\pi}{b}(y' + \frac{b}{2})\right) + \sum_{n=0}^N \beta_{mn}^y \cos\left(\frac{n\pi}{b}(y' + \frac{b}{2})\right) \right) \sin\left(\frac{m\pi}{a}(x' + \frac{a}{2})\right) \right] \right\} e^{j(k_x x' + k_y y')} dx' dy' \right| \quad (11b)$$

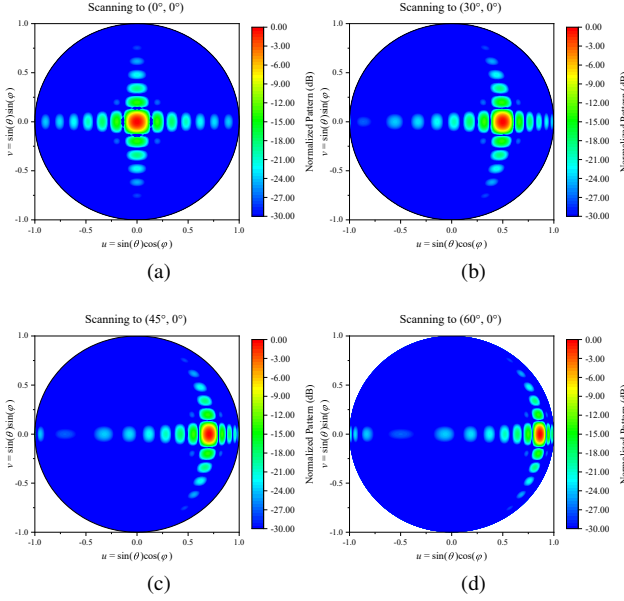


Fig. 2. Target radiation pattern scanning to different angles. (a) Scanning to \$(0^\circ, 0^\circ)\$; (b) Scanning to \$(30^\circ, 0^\circ)\$; (c) Scanning to \$(45^\circ, 0^\circ)\$; (d) Scanning to \$(60^\circ, 0^\circ)\$.

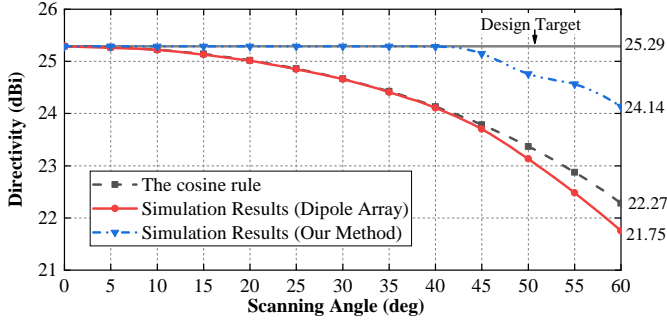


Fig. 3. Comparison of directivity of the cosine rule, dipole array, and the aperture field we designed.

VI. CONCLUSION

A method for designing aperture field from an arbitrary phaseless pattern is proposed in this communication. This method has strong universality and can deal with the non-linearity introduced by phaseless. We give the derivation of the method, the analytical expression of the integral equation

and the parameter values. And successfully use this method to design a set of aperture field that could break the cosine rule.

There is still much follow-up work to be done, such as what the bounds of achievable radiation pattern complexity with finite apertures are, how to physically implement the aperture field and so on.

APPENDIX A

ANALYTICAL EXPRESSION OF EQUATION (11)

Equation (15) is the analytic expression of Equation (11).

$$f_x(\theta, \phi) = \sum_{n=1}^N \left(\sum_{m=1}^M \alpha_{mn}^x \prod_{i=1}^3 g_{1,i}(m, n, \theta, \phi) + \sum_{m=0}^M \beta_{mn}^x \prod_{i=1}^3 g_{2,i}(m, n, \theta, \phi) \right) \quad (15a)$$

$$f_y(\theta, \phi) = \sum_{m=1}^M \left(\sum_{n=1}^N \alpha_{mn}^y \prod_{i=1}^3 g_{1,i}(m, n, \theta, \phi) + \sum_{n=0}^N \beta_{mn}^y \prod_{i=1}^3 g_{3,i}(m, n, \theta, \phi) \right) \quad (15b)$$

where the $g_{j,i}$ are defined in (16).

$$\chi_1 = \sin \theta \sin \phi \quad (16a)$$

$$\chi_2 = \sin \theta \cos \phi \quad (16b)$$

$$g_{1,1} = \left(4abe^{-\frac{1}{2}jk\cos\phi(b\cos\theta+a\sin\theta)} \times \left[(4n^2\pi^2 + b^2k^2(\cos(2\phi) + 2\cos(2\theta)\sin^2(\phi) - 1)) \times (a^2k^2\chi_2^2 - m^2\pi^2) \right]^{-1} \right) \quad (16c)$$

$$g_{1,2} = (-m\pi + e^{jkax_2}(m\pi \cos(m\pi) - jbk \sin(m\pi)\chi_2)) \quad (16d)$$

$$g_{1,3} = \left(e^{\frac{1}{2}jkb\cos(\phi+\theta)n\pi} + e^{\frac{1}{2}jkb\cos(\phi-\theta)n\pi} (-n\pi \cos(n\pi) + jbk \sin(n\pi)\chi_1) \right) \quad (16e)$$

$$g_{3,1} = g_{2,1} = g_{1,1} \quad (16f)$$

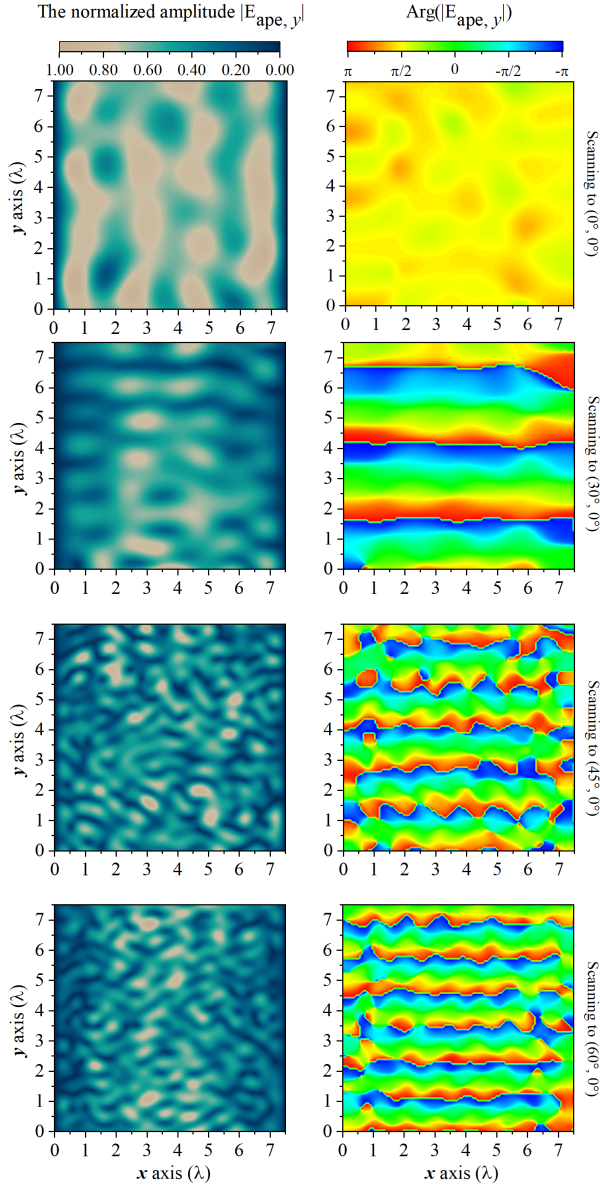


Fig. 4. The normalized amplitude distribution and phase distribution of aperture field obtained by inverse design.

$$g_{2,2} = \left(-ak\chi_2 + e^{jk\alpha\chi_2} (-jm\pi \sin(m\pi) + ak \cos(m\pi) \chi_2) \right) \quad (16g)$$

$$g_{2,3} = -jg_{1,3} \quad (16h)$$

$$g_{3,2} = \left(-jm\pi + e^{jk\alpha\chi_2} (jm\pi \cos(m\pi) + ak \sin(m\pi) \chi_2) \right) \quad (16i)$$

$$g_{3,3} = \left(-bk\chi_1 e^{\frac{1}{2}jkb \cos(\phi+\theta)} + e^{\frac{1}{2}jkb \cos(\phi-\theta)} (-jn\pi \sin(n\pi) + bk \cos(n\pi) \chi_1) \right) \quad (16j)$$

REFERENCES

[1] L. A. Bronckers, A. Roc'h, and A. B. Smolders, "A new design method for frequency-reconfigurable antennas using multiple tuning

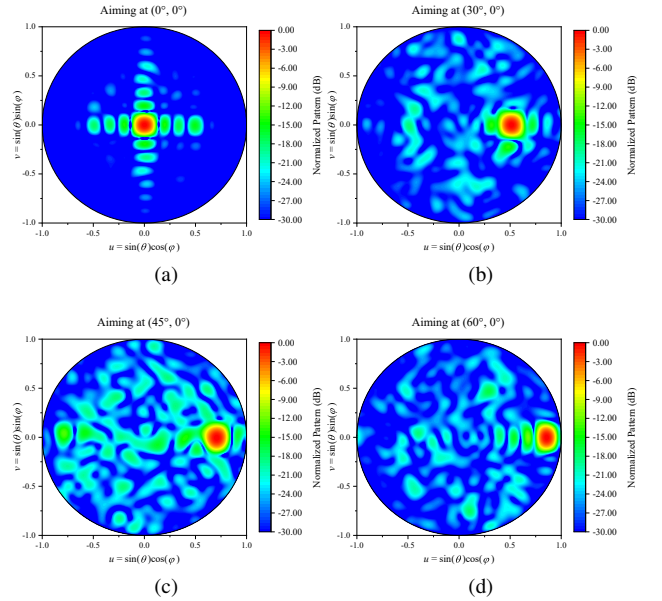


Fig. 5. The radiation pattern of aperture field designed by this method with different scanning angles. (a) Aiming at $(0^\circ, 0^\circ)$; (b) Aiming at $(30^\circ, 0^\circ)$; (c) Aiming at $(45^\circ, 0^\circ)$; (d) Aiming at $(60^\circ, 0^\circ)$.

components," *IEEE Transactions on Antennas and Propagation*, vol. 67, no. 12, pp. 7285-7295, Dec. 2019.

- [2] Y. Liu, Y. Jia, W. Zhang, Y. Wang, S. Gong, and G. Liao, "An integrated radiation and scattering performance design method of low-RCS patch antenna array with different antenna elements," *IEEE Transactions on Antennas and Propagation*, vol. 67, no. 9, pp. 6199-6204, Sep. 2019.
- [3] X. Huang, Y. Liu, P. You, M. Zhang, and Q. H. Liu, "Fast linear array synthesis including coupling effects utilizing iterative FFT via least-squares active element pattern," *IEEE Antennas and Wireless Propagation Letters*, vol. 16, pp. 804-807, Aug. 2017.
- [4] R. Bera, D. Mandal, R. Kar, and S. P. Ghoshal, "Non-uniform single-ring antenna array design using wavelet mutation based novel particle swarm optimization technique," *Computers & Electrical Engineering*, vol. 61, pp. 151-172, Jul. 2017. [Online]. Available: <https://www.sciencedirect.com/science/article/pii/S0045790617312569>
- [5] N. K. Nikolova, *Introduction to Microwave Imaging*, ser. EuMA High Frequency Technologies Series. Cambridge University Press, Jul. 2017.
- [6] S. Molesky, Z. Lin, A. Y. Piggott, W. Jin, J. Vucković, and A. W. Rodriguez, "Inverse design in nanophotonics," *Nature Photonics*, vol. 12, no. 11, pp. 659-670, Nov. 2018.
- [7] Z. Wei and X. Chen, "Physics-inspired convolutional neural network for solving full-wave inverse scattering problems," *IEEE Transactions on Antennas and Propagation*, vol. 67, no. 9, pp. 6138-6148, Sep. 2019.
- [8] M. Salucci, A. Gelmini, G. Oliveri, N. Anselmi, and A. Massa, "Synthesis of shaped beam reflectarrays with constrained geometry by exploiting nonradiating surface currents," *IEEE Transactions on Antennas and Propagation*, vol. 66, no. 11, pp. 5805-5817, Nov. 2018.
- [9] T. Brown, C. Narendra, Y. Vahabzadeh, C. Caloz, and P. Mojabi, "On the use of electromagnetic inversion for metasurface design," *IEEE Transactions on Antennas and Propagation*, vol. 68, no. 3, pp. 1812-1824, Mar. 2020.
- [10] C. Narendra, T. Brown, and P. Mojabi, "Gradient-based electromagnetic inversion for metasurface design using circuit models," *IEEE Transactions on Antennas and Propagation*, vol. 70, no. 3, pp. 2046-2058, Mar. 2022.
- [11] R. Fletcher and C. M. Reeves, "Function minimization by conjugate gradients," *The Computer Journal*, vol. 7, no. 2, pp. 149-154, Jan. 1964. [Online]. Available: <https://doi.org/10.1093/comjnl/7.2.149>
- [12] A. Taaghool and T. Sarkar, "Near-field to near/far-field transformation for arbitrary near-field geometry, utilizing an equivalent magnetic current," *IEEE Transactions on Electromagnetic Compatibility*, vol. 38, no. 3, pp. 536-542, Aug. 1996.
- [13] M. Sørensen, H. Kajbaf, V. V. Khilkevich, L. Zhang, and D. Pommerenke, "Analysis of the effect on image quality of different scanning

- point selection methods in sparse esm," *IEEE Transactions on Electromagnetic Compatibility*, vol. 61, no. 6, pp. 1823–1831, Dec 2019.
- [14] D. Yuan and X. Zhang, "An overview of numerical methods for the first kind Fredholm integral equation," *SN Applied Sciences*, vol. 1, no. 10, p. 1178, Oct. 2019. [Online]. Available: <https://doi.org/10.1007/s42452-019-1228-3><http://link.springer.com/10.1007/s42452-019-1228-3>
- [15] N. Liu, S.-W. Qu, Y. Ma, and S. Yang, "Irregular phased array architecture with small directivity drop for wide-angle scanning application," *IEEE Transactions on Antennas and Propagation*, pp. 1–1, 2022.